

Aerodynamic design of a Martian micro air vehicle

Hervé Bézard, Thibault Désert*, Jean-Marc Moschetta** and Thierry Jardin***

**ONERA, Department of MultiPhysics for Energetics*

2, av. E. Belin, F-31055 Toulouse, France. herve.bezard@onera.fr

***ISAE-SUPAERO - Department of Aerodynamics, Energetics and Propulsion*

10, av. E. Belin, F-31055 Toulouse, France. jean-marc.moschetta@isae-supaeero.fr

Abstract

This paper presents a numerical and experimental study of the aerodynamic characteristics of a VTOL micro air vehicle designed to fly on Mars. A blade airfoil is optimized for compressible and ultra-low Reynolds number flows. It is evaluated using unsteady laminar Navier-Stokes simulations. Isolated and coaxial rotors are designed using a free wake lifting line method and are evaluated using Navier-Stokes solvers. Optimized rotors are evaluated experimentally in the ONERA's low pressure tank, recreating Martian atmosphere. A set-up developed by ISAE-SUPAERO provides thrust and torque measurements, up to blade tip transonic flow conditions.

1. Introduction

The exploration of the surface of Mars is made by rovers, such as Curiosity or Opportunity, which are limited in terms of range and accessibility. Only 60 km were explored on the 21 000 km of the planet's circumferential path. Slow exploration rate is mainly due to the hilly landscape implying a limited traversable terrain and a lack of visibility on the ground. An aerial vehicle associated to a rover could significantly increase the global range and mobility by providing an aerial point of view of its upcoming pathway.

A fixed-wing aircraft has the ability to map a large geographical area. However, it needs to fly fast enough to compensate the very low density of Mars' atmosphere, which limits its maneuverability. It can hardly take-off from and land on the rocky ground of Mars, which limits its mission to one flight, as in the ARES project of NASA [4]. A balloon is a compromise between aircraft and orbiters. It can stay several days at a few kilometers altitude covering thousands of kilometers of varied terrain [11]. Since balloon movement depends on atmospheric flows, the range of manoeuvres is limited and a balloon is very sensitive to the severe winds blowing on Mars. Vertical take-off and landing (VTOL) micro-aerial vehicles (MAV) seem the best suited aircraft for this mission compared to fixed wing aircraft or balloons. Such a drone could be able to fly over the terrain around the rover to prepare its future paths, but also to explore inaccessible places such as cliffs and canyons, and even land on the ground to retrieve small samples of soil and get back to the rover for analysis. This advanced and original concept is studied in different countries (USA, Japan, China, Europe) and space research institutes (NASA, JAXA). The NASA/JPL is currently working on a Martian helicopter for the Mars 2020 launch [1]. It is made of 1.2 m diameter coaxial rotors and weighs 1.8 kg. Its energy comes from a small solar panel on top of it, which limits its flight to less than 2 min per day.

In the present paper, a smaller vehicle is proposed, typically 30 cm diameter, which could be easily packed and protected inside the rover. The small dimensions could facilitate swarming, maneuverability and interactions with rovers and, in a potential future, with humans. Such a MAV could land/take-off on or close to the rover, recharge and heat its batteries and exchange data collected in flight directly on the rover or by means of a dedicated robotic arm. Because of the Martian atmosphere's characteristics, rotor blades spin in compressible and ultra-low Reynolds number conditions. This is a new and little explored domain of aerodynamics, with very few numerical and experimental data available. Designing an efficient rotorcraft for these conditions is very challenging. Optimization of airfoil and rotor blade geometries is necessary to achieve sufficient thrust with minimum power for an instrumented Martian flight. In the literature, isolated rotor blade shape optimization based on the blade element momentum theory (BEMT) was achieved for $Re_c < 10^4$ by Kunz [12], Liu [16] and Bohorquez [3]. Airfoils were designed either by simple panel method coupled with integral boundary layer method (XFOIL [9]), or by incompressible Navier-Stokes code (INS2D [19]). For its Mars' helicopter, NASA [1] used a free vortex method

(FVM) to optimize the planform distribution of the two-bladed coaxial rotors. The coaxial rotor configuration is proven to be the most efficient propulsion system for a given size [20].

Ultra-low Reynolds number conditions can be found on nanorotors at ambient pressure or recreated in depressurized facilities. Bohorquez [3] assessed the performance of isolated nano rectangular blades for $Re_c < 10^4$, and the impact of spacing between upper and lower rotor in a coaxial configuration. Other studies evaluated the influence of coaxial rotors' spacing in low Reynolds number flows through simulations [13] and experiments [17]. As for isolated rotors in depressurized facilities, NASA first experimented a four bladed rotor with linear twist distribution [23]. The experiment was simulated in 3D to investigate the flow behavior for a tip Reynolds number $Re_{tip} > 6.10^4$ [6]. In the range $Re < 10^4$, the influence of span, curvature, taper, Reynolds number, blade incidence and rotation speed were experimentally measured in other depressurized facilities [20][21][22].

There are still many points to address. BEMT and FVM have not been validated in compressible ultra-low Reynolds flows contrarily to high fidelity solvers. No optimization of the full propulsion system based on FVM has been carried out for now. No study provides 3D validated CFD simulations of the experimentally evaluated rotors in the range of Reynolds number of the Martian MAV corresponding to fully laminar flows. Experiments have not been carried out up to transonic conditions at blade tip. This paper proposes to complete this missing information. After a brief presentation of Mars atmosphere characteristics and aerodynamic conditions for the blade flow, Navier-Stokes solver is validated on a referenced experiment from literature. The optimization of the blade airfoil is then presented and performance is evaluated with the validated solver for a large range of Mach and Reynolds numbers. Isolated rotor geometries are optimized using BEMT or FVM, and a lower rotor coaxial configuration is optimized taking into account the interaction with the upper rotor wake. Geometries are investigated numerically with the Navier-Stokes solver. Experiments carried out in the ONERA's low pressure tank are presented, with both thrust and torque measurements, for isolated and coaxial configurations, for a large range of rotation speeds. The paper concludes on the feasibility of a Martian MAV and gives some perspectives for future studies.

2. Martian atmosphere and aerodynamic conditions

The main drawback of Mars' atmosphere in terms of flight capability is the extreme low density: about one hundred times lower than on Earth. During daytime, it can fluctuate between 0.014 and 0.020 kg/m³ [1]. As seen in Table 1, that compares the average characteristics of Earth's and Martian atmospheres, Martian equivalent conditions can be found on Earth in the stratosphere at an altitude of about 30 km. One can easily imagine that flying a VTOL MAV at such an altitude on Earth is very challenging. Martian atmospheric temperature, strongly controlled by suspended dust holding solar radiations, is also lower than on Earth and eminently variable with 60 °C of diurnal near-surface range [15]. The low temperature combined with a low specific heat ratio (Martian atmosphere is composed of 96% of carbon dioxide CO₂) directly lowers the speed of sound. This gives a compressible aspect of the flow around the blades, especially if high rotation speed is needed. Despite these drawbacks, an advantage on Mars is the low gravity, which is about two and a half times lower than on Earth. The viscosities are quite comparable between Mars and Earth, which means that the low Reynolds numbers come mainly from the low density. It is worth to note that Mars' atmosphere is very turbulent, with strong winds and dust storms. This is a key point to take into account when designing for stability and operability of a Martian MAV.

Table 1: Average characteristics of Earth's and Martian atmospheres

	Earth (ground)	Mars (ground)	Earth (30 km)
Gravity (m/s ²)	9.81	3.72	9.78
Density (kg/m ³)	1.225	0.0167	0.0177
Temperature (°C)	15	-63	-46
Pressure (Pa)	10 ⁵	660	1150
Dynamic viscosity (Pa.s)	1.8 10 ⁻⁵	1.06 10 ⁻⁵	1.47 10 ⁻⁵
Sound velocity (m/s)	340	230	300
Specific heat ratio	1.4	1.34	1.4

Because of the very low density and the small size of the vehicle, one may rightly question about the continuum aspect of the flow around the blades. This point can be addressed through the Knudsen number, which can be expressed as: $Kn = M\sqrt{(\gamma\pi/2)}/Re$, where M is the Mach number, Re the Reynolds number and γ the specific heat ratio. Even for a transonic flow at $M = 0.7$ and ultra-low Reynolds number of 1000, Knudsen number is 0.001, which is far

below the 0.1 value considered as the limit for continuum physics. This confirms that traditional aerodynamics based on Navier-Stokes equations applies.

As mentioned above, the MAV rotor dimension considered here is 30 cm. Simulations are performed in Martian conditions with the daytime minimal density value of 0.014 kg/m^3 and the speed of sound average value of 230 m/s. A parametric study made previously [2] shows that the mass lift by an isolated hovering rotor lies between 100 g and 300 g only, taking into account the limit of 0.7 for the maximum tip Mach number (obtained at a rotation speed of 10 000 rpm) to avoid strong transonic phenomena on the blades and consequent power penalty due to shock waves. In Martian gravity, the corresponding thrust lies between 0.37 N and 1.1 N. For chord values lower than 10 cm, Reynolds numbers are below 10^4 . To know if the boundary layer over airfoils is laminar or turbulent, linear stability analyses were performed on two different airfoils at $Re = 6000$ and $M = 0.5$ [7]. The calculated N factor (e^N method) is always below 1, which proves the flow is fully laminar.

3. Numerical validation of unsteady laminar Navier-Stokes simulations

As mentioned previously, the flow around blades is laminar for $Re_c < 10^4$. It is also known that laminar boundary layer separation easily occurs on cambered airfoils, even at moderate angle of attack, and evolves rapidly in unsteady flow. Unsteady laminar Navier-Stokes solver seems to be the better method to evaluate airfoils and blades in Martian conditions. Simulating both laminar and compressible flow around geometries is however unusual and the solver needs to be validated before. The ONERA's Navier-Stokes code named *elsA* [5] is used here. It is based on an integral form of the compressible Navier-Stokes equations. Simulations performed on a same test case with another Navier-Stokes code (*STAR-CCM+*) give very comparable results for both codes (not presented here).

The *Mars Wind Tunnel* (MWT), located at Tohoku University, is a depressurized facility reaching Martian density for different Mach numbers (see Figure 1 (left)). For validation purpose, the triangular airfoil experiment [18] is considered. This airfoil's strong leading edge camber and sharpness causes significant unsteadiness in the flow, making it interesting for numerical validation. MWT experiment is supposed to recreate 2D flows. However, pressure sensitive paint (PSP) measurements show the three-dimensionality of the flow over the airfoil caused by the influence of the side walls of the test section. Therefore, structured 3D grids are created around the airfoil and include all wind tunnel's walls. Three angles of attack are considered for the simulations: 5° , 10° and 15° . 2D H-grids are first created with 240 cells mapping the airfoil's upper surface and 150 for the lower surface. 3D grids are generated from 2D grids with 130 cells in the spanwise direction for a width of 3.3 chords, with a total of 15 million cells. Grid convergence was checked for each Navier-Stokes simulation.

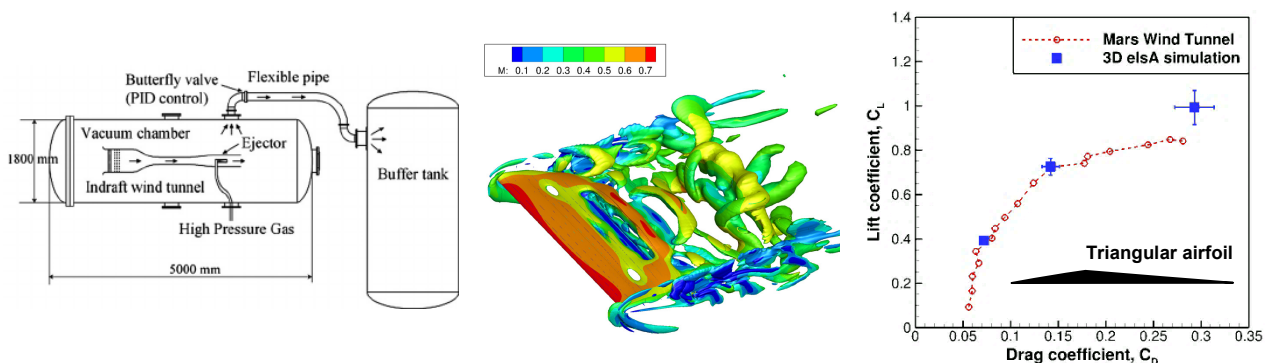


Figure 1: Validation of 3D unsteady laminar *elsA* simulations. (left) Mars Wind Tunnel facility of Tohoku University [18]. (middle) Q-criterion iso-surfaces colored by Mach number ($AoA = 10^\circ$). (right) Lift and drag coefficients ($Re_c = 3000$, $M = 0.5$).

Present 3D numerical simulations corroborate the three-dimensionality of the flow in the facility, as seen in Figure 1 (middle) that plots the Q-criterion's iso-surfaces for $Re_c = 3000$, $M = 0.5$ and $AoA = 10^\circ$. Unsteady laminar Navier-Stokes solver perfectly predicts the 3D lift and drag coefficients (respectively C_L and C_D) generated at the two first angles of attack (5° and 10°) as shown in Figure 1 (right). At $AoA = 15^\circ$, corresponding to a fully detached flow, computed lift is slightly over-estimated. However, in the present study, airfoil aerodynamic performance is compared in the most effective range of angles of attack, i.e. when the flow is not fully separated. Therefore, the solver is validated for 3D flows and should also provide reliable 2D predictions.

4. Airfoil optimization based on Xfoil's performance evaluations

A complete rotor shape could be directly optimized by 3D Navier-Stokes simulations. However, the number of parameters describing the geometry can be very important and would involve a great computational and meshing effort. It was decided to split the rotor design into firstly, the airfoil design (camber and thickness distributions) and secondly, the blade design (chord and twist distributions). Designing the airfoil is possible again by Navier-Stokes simulations. For the same reason, a simpler aerodynamic evaluation based on Xfoil [9] is used. Xfoil is a 2D high order panel method fully coupled with an integral boundary layer method. Compressibility is taken into account through Kármán-Tsien corrections. This tool was compared with *elsA* Navier-Stokes code in [8] and it was shown that for the most performant aerodynamic conditions, that is non-fully separated flow, both codes give similar results for 10^8 times lower computational effort with Xfoil. Xfoil still compares well with steady Navier-Stokes simulations for higher angles of attack where limited trailing edge flow separation occurs, but it is no more in agreement when the flow's unsteadiness is important, e.g. when fully separated flow occurs. In these conditions, the unsteady laminar Navier-Stokes simulations, which were proven previously to be the more relevant, provide much higher lift than Xfoil.

In a purpose of optimization, automatic airfoil generation with finite parameters is essential. The parameterization method based on Class-Shape function Transformation (CST) was chosen for its ability to recreate any C^2 continuous airfoil shapes with a restricted number of parameters. In this study, five parameters are used to reflect the shape of the camber or thickness distribution. The objective of the optimization is to produce maximum lift with minimum drag, which is equivalent to maximizing the lift-to-drag ratio C_L/C_D . But the objective can also be maximizing $C_L^{3/2}/C_D$, which is linked to the range of an aircraft. The best is to combine both in a unique objective function. Because aerodynamic conditions are not accurately known and to avoid a too sharp design, the airfoil has to be efficient over a large range of Reynolds number and angles of attack. The final objective function is thus an average of the sum $C_L/C_D + C_L^{3/2}/C_D$ over four angles of attack around the optimum, and an average over three Reynolds numbers: 2000, 6000 and 10 000. The optimization process consists in evaluating the entire parameter domain with an increasing proximity between the different sets of parameters. This demands a very important number of set evaluations. Approximately half a million Xfoil evaluations are carried out for one optimization. Different optimizations are performed, from incompressible to compressible one, from thickness or camber separate optimizations to both camber and thickness optimization. Finally, the compressible thickness and camber optimized airfoil, which is the most performant, is kept for the rotor design.

5. Navier-Stokes evaluations of the optimized airfoil

As an example, Figure 2 shows the instantaneous flow (*elsA* unsteady laminar simulations) around the optimized airfoil at $Re_c = 6000$, $M = 0.5$, for an angle of attack of 6° where the flow is attached on most of the chord and of 8° where the flow is separated. The optimized airfoil has a quasi-constant thickness (about 2% chord) and a high camber (about 6% chord), with rounded trailing edge. The leading edge's camber allows the flow to adapt at high angle of attack and limits the acceleration to prevent separation. The trailing edge's camber allows the laminar separation to occur as downstream as possible to limit the pressure drag in this region. It can be noticed that the large boundary layer thickness is due to ultra-low Reynolds number conditions. At $AoA = 8^\circ$, even if the flow is separated, the mean lift coefficient C_{Lmean} is still high (1.45) compared to its value at $AoA = 5^\circ$ (0.95) where the flow is attached. This behavior comes from vortices periodically forming at the leading edge and staying close to the upper surface before advecting away from the airfoil, thus producing high local velocities and low local pressures that explain an over-production of lift on the upper side.

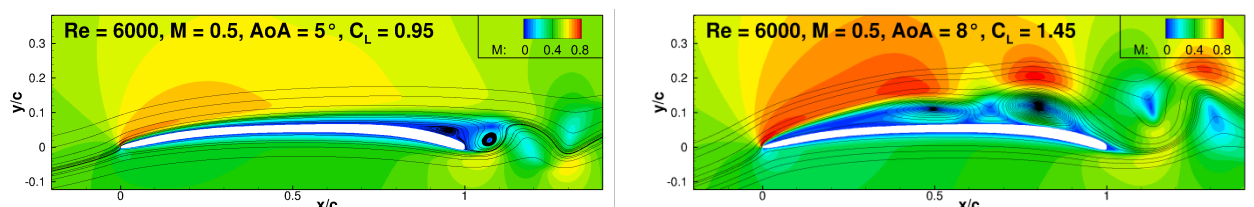


Figure 2: Unsteady laminar Navier-Stokes simulations (*elsA*) for optimized airfoil. Mach number contours at $Re_c = 6000$ and $M = 0.5$. (left) $AoA = 5^\circ$, $C_{Lmean} = 0.95$. (right) $AoA = 8^\circ$, $C_{Lmean} = 1.45$.

The optimized airfoil is fully evaluated through unsteady laminar Navier-stokes simulations with *elsA* over a large range of Reynolds numbers, Mach numbers and angles of attack to provide the necessary data base for the rotor optimization.

Figure 3 shows the effect, on the flow and on the aerodynamic coefficients, of the Reynolds number at a given Mach number of 0.5. The lift coefficient and the lift-to-drag ratio are strongly dependent on the Reynolds number (Figure 3). At $Re_c = 10\,000$, the maximum lift-to-drag ratio is only 15, compared to 100 to 200 for classical airfoils at high Reynolds number. C_L/C_D falls to 5 at $Re_c = 1000$ because boundary layers are very thick, as seen on the corresponding flow on the left of Figure 3. The lift coefficient of maximum performance is always close to 1. The break visible for $C_L > 1$ and for Re_c values greater than 3000 is due to the occurrence of separated flow, as seen previously in Figure 2. At these very low Reynolds numbers, the lift coefficient still increases at high angles of attack and no stall occurs. A C_L of 2 is almost reached at 15° angle of attack for the highest Reynolds number values.

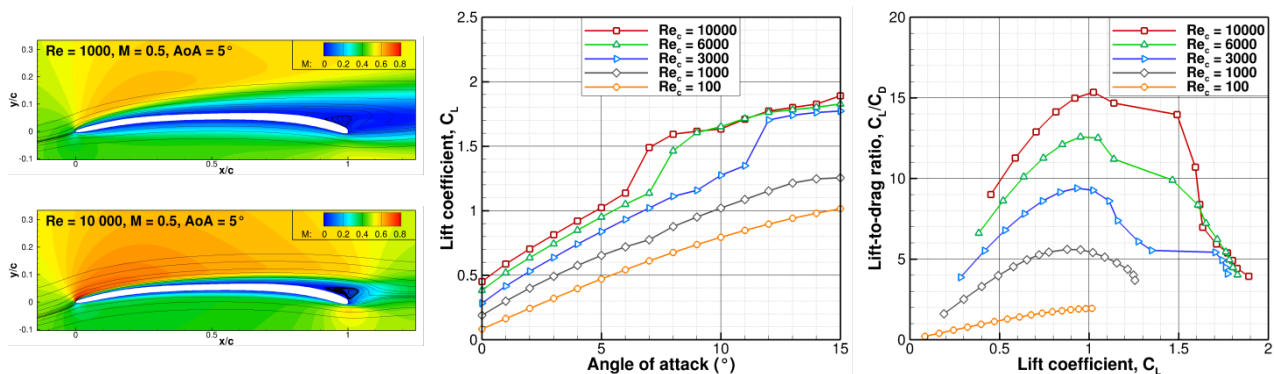


Figure 3: Effect of Reynolds number at $M = 0.5$. Unsteady laminar Navier-Stokes simulations (*elsA*). (left) Average Mach number contours. (middle) Lift coefficient vs angle of attack. (right) Lift-to-drag ratio vs lift coefficient.

Figure 4 shows the effect of the Mach number at a given Reynolds number of 3000. The C_L increases with the Mach number, except at $M = 0.9$ where a large separation occurs (not shown here). The C_L/C_D is almost independent of the Mach number up to $M = 0.7$. But for $M > 0.7$, the performance decreases rapidly with the Mach number, due to the occurrence of supersonic regions and shock waves, as seen on the corresponding flow at $M = 0.8$. $M = 0.7$ is the divergence drag Mach number and should be considered as a limit for the blade tip Mach number, which gives a maximum rotation speed of about 10 000 rpm in Martian conditions for a rotor diameter of 30 cm.

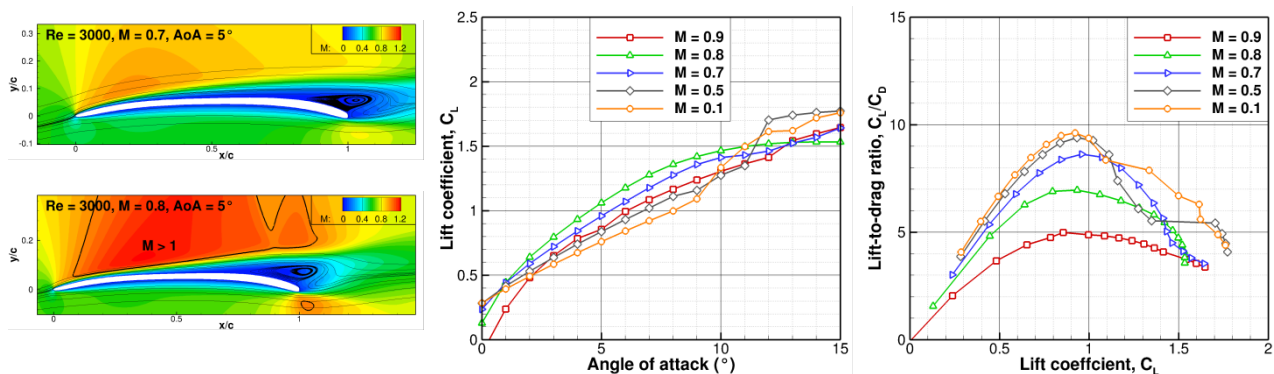


Figure 4: Effect of Mach number at $Re = 3000$. Unsteady laminar Navier-Stokes simulations (*elsA*). (left) Average Mach number contours. (middle) Lift coefficient vs angle of attack. (right) Lift-to-drag ratio vs lift coefficient.

6. Evaluation of simpler numerical solvers for performance evaluation of rotors in hover

As already discussed before, using 3D unsteady Navier-Stokes simulations for rotor optimization is time consuming and simpler methods are preferred, on the condition that they give accurate enough results. Two low-computational cost solvers are evaluated here: one based on the Blade Element Momentum Theory (BEMT), named QMIL/QPROP developed by Drela [10], the second based on the Free Vortex Method (FVM), named PUMA and developed by

ONERA, which combines a lifting line approach and a free wake model. Both methods rely on airfoil aerodynamic characteristics given here by 2D unsteady laminar Navier-Stokes simulations. A three-blade rotor was designed using BEMT (QMIL) by minimizing induced loss. The chords are reduced in the root region for no overlapping of the blades at hub. The planform is visible in Figure 5.

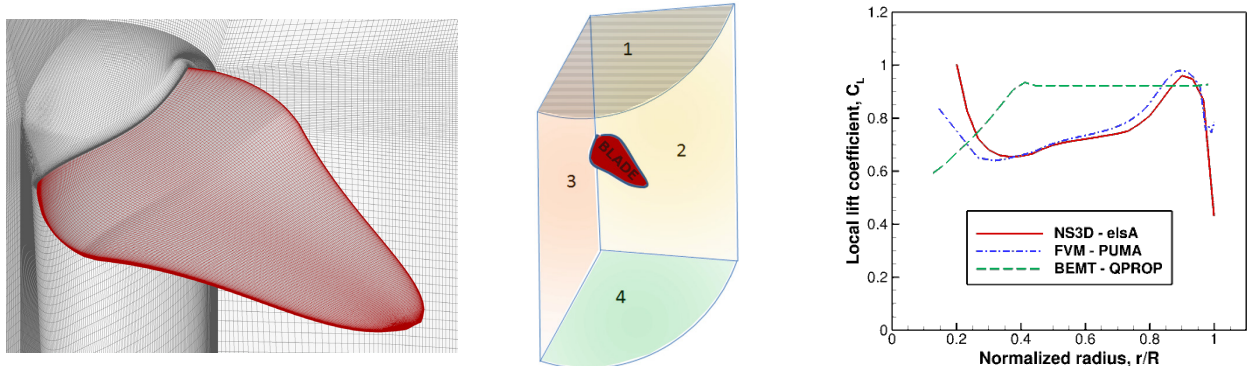


Figure 5: Evaluation of numerical solvers on BEMT optimized rotor. (left) Grid for Navier-Stokes simulations. (middle) Domain boundaries. (right) Local lift coefficient distributions vs span location at $\Omega = 7500$ rpm.

Numerical evaluations are performed on the BEMT-optimized rotor. For Navier-Stokes simulations, only a third of the domain is simulated with a periodic condition (sides 2 and 3, Figure 5) for blade-to-blade interactions, with a 13 million cells structured grid. For convergence facilitation, a velocity field based on Froude theory is implemented through upper and lower domain's boundaries (sides 1 and 4, Figure 5). The local lift coefficient distributions along the span are compared in Figure 5, for a rotation speed Ω of 7500 rpm and a total thrust of 0.37 N in Martian conditions. FVM and Navier-Stokes results are close, which is not the case for BEMT results. The main difference between FVM and BEMT is the modeling of the wake. In PUMA (FVM), the free wake model allows a better estimation of the local induced angles, as in Navier-Stokes simulation. In terms of computational cost, BEMT simulations are almost instantaneous ($\sim 10^{-5}$ h). FVM simulations take more time to converge ($\sim 10^{-2}$ h), which is however five orders of magnitude lower than Navier-Stokes' computational cost ($\sim 10^3$ h). FVM provides accurate results for acceptable computational time and is thus adequate for rotor optimization.

7. Isolated and coaxial rotor optimization based on FVM's performance evaluations

Optimal rotor blades have nearly equal Reynolds number distribution along the span, compensating local speed variation with chord length. Therefore, in a non-constrained optimization process, chord length tends to infinity at blade root. In order to optimize a realizable rotor shape, blade root distribution has to be constrained. No-overlapping condition is not sufficient since optimized root-twist tends to a large value and rotor shape tends to a non-feasible and non-optimal rotor in terms of mass. For manufacture feasibility and structural robustness, blade root twist is set to zero. Corresponding chord length is calculated in agreement with the no-overlapping constraint. Since most of rotor thrust is generated by the blade tip area, a constrained blade root distribution allows restricting rotor weight in the most inefficient part of the blade. Rotors are made of three blades, an odd number, to avoid specific vibration axes. In a purpose of optimization, automatic rotor shape generation with finite parameters is essential. Spline representation with five control points is used to generate the shape of the chord or twist distributions. The optimization process consists in evaluating the entire parameter domain with an increasing proximity between the different sets of parameters, as in the 2D optimization.

The present study aims at building a propulsion system able to sustain 200 g in hover in the Martian atmosphere (thrust $T = 0.74$ N). First step is to optimize an isolated rotor generating a thrust of 100 g ($T = 0.37$ N). Then, for coaxial configuration optimization, the optimized isolated rotor is used as the upper rotor. The lower rotor is optimized for generating the remaining 100 g of thrust while cancelling the residual torque Q of the coaxial propulsion system, with no constraint on the rotation speed. Releasing the constraint on the lower rotor's rotation speed allows the lower rotor to rotate faster and to have smaller chords, and thus lower mass. The influence of upper rotor's induced velocity and vorticity is taken into account thanks to the free wake model. The lower rotor is assumed to have little impact on the upper rotor. Coaxial rotors' spacing is set to $h = 0.08$ m ($h/R \sim 0.5$) for lower rotor optimization. For $h/R > 0.4$, it was shown [3][13] that the spacing between coaxial rotors has little impact on global performance.

In the optimization process based on FVM (PUMA), each rotor's rotating speed corresponding to $T = 0.37$ N in Martian conditions is obtained from three solver evaluations at different rotating speeds. Values are interpolated assuming thrust and torque are functions of Ω^2 . More than 30 000 isolated upper rotor and 6000 lower rotor geometries were evaluated with the FVM solver.

The three-blade upper and lower rotors showing the lowest power consumption for a 2×0.37 N thrust generation are presented in Figure 6. Twist values at the spline's control points are also indicated. The upper and lower rotors rotate respectively at 6100 rpm and 8500 rpm. The upper rotor's optimized shape is highly twisted and elliptic. On the contrary, the lower rotor's shape is slimmer in the central section of the blade and is larger in the outer part. Both twist distributions are close. Note that for both rotors, twist is low ($\beta = 2^\circ$) at blade tip for tip vortices reduction. The local thrust distributions along the span evaluated by the FVM solver for both rotors are presented in Figure 6. For the lower rotor, a lot of thrust is produced in the outer part of the blade to take advantage of the non-disturbed flow due to the upper wake contraction, which explains the larger chords in this region compared to the central one where the upper wake induced velocities allow the chords to be reduced.

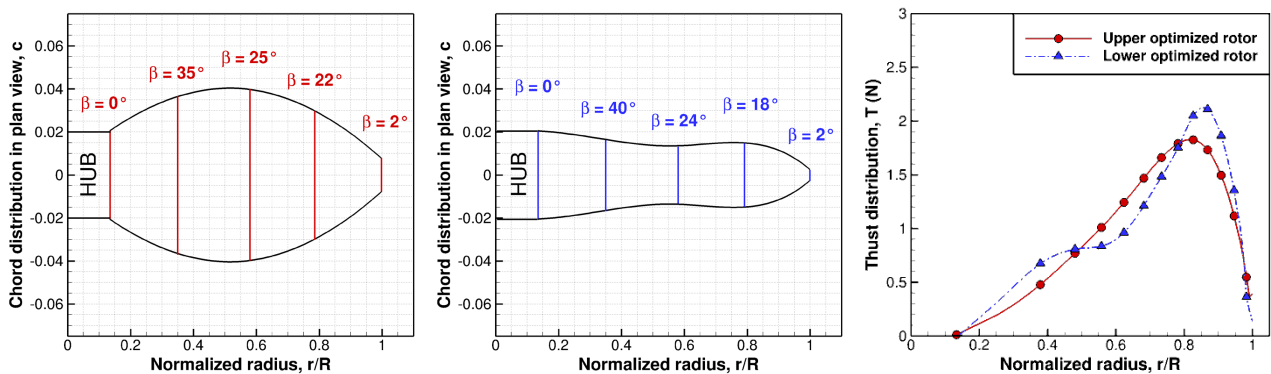


Figure 6: FVM-optimized coaxial configuration (2×0.37 N total thrust). (left) Lower rotor shape ($\Omega_{0.37N} = 6100$ rpm). (middle) Upper rotor shape ($\Omega_{0.37N} = 8500$ rpm). (right) Local thrust distributions vs span.

8. Navier-Stokes evaluation of coaxial rotor configuration

Isolated and coaxial rotors are evaluated by the validated Navier-Stokes solvers. *elsA* and *STAR-CCM+* are both used for isolated rotors, but only the second solver is used for the coaxial configuration, due to its simpler implementation and unstructured meshing tool. The isolated upper rotor was evaluated with both codes and results were completely similar. The isolated upper rotor is not presented here but, as it was mentioned previously, it behaves almost identically when isolated or when placed in the coaxial configuration. Only the results of the coaxial configuration are thus presented below in Figure 7. The grid has 26 million cells.

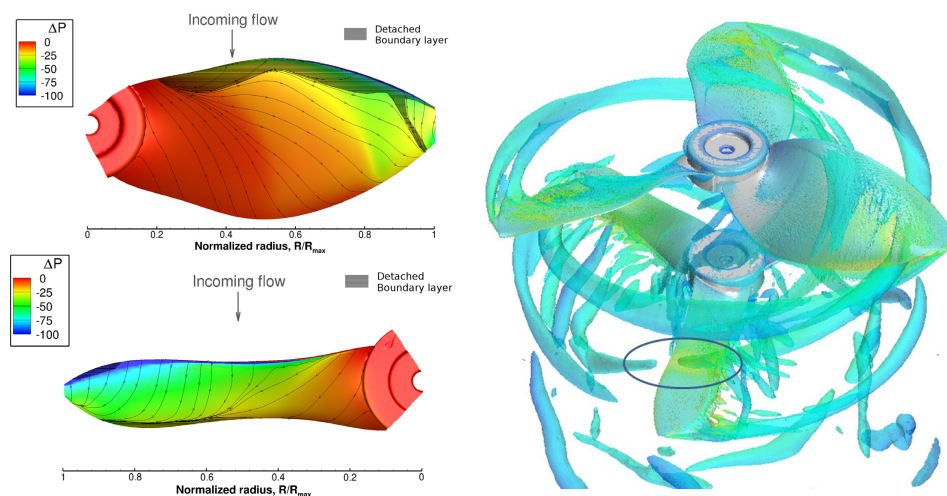


Figure 7: Unsteady laminar Navier-Stokes simulation of coaxial configuration for 0.74 N total thrust. (left) Surface pressure and friction lines with separated regions. (right) Contours of Q-criterion colored by velocity.

The wall pressure and friction lines on the upper side of the upper and lower rotors are shown in Figure 7. The friction lines' curvature shows that the boundary layer flow is strongly three-dimensional, especially on the upper rotor which has a low aspect ratio. The separated areas are also shaded in the figure. A stable leading edge vortex (LEV) is seen at the upper rotor's leading edge, which leaves the surface close to the tip. It merges with the tip vortex, as seen in Figure 7 which shows the vortices through the Q-criterion. This LEV was not expected as the FVM solver is not able to reproduce this phenomenon, but it seems to have low impact on the performance. On the lower rotor, the flow is less three-dimensional, due to the higher aspect ratio of the blade, especially in the outer part where a separated region corresponding to the 2D flow separation at the airfoil trailing edge occurs. The upper rotor tip vortex impacts the lower rotor at about 70% span, corresponding to the region where the local thrust is lowered (see the circle in Figure 7). The FVM solver is able to capture this interaction and the optimization process was able to minimize its impact on the overall performance.

9. Experimental evaluation of optimized rotors in low density conditions

To validate the results of the optimization process, optimized rotors are evaluated experimentally in conditions close to the Martian ones. ONERA's low pressure tank (see Figure 8), which has a volume of 18 m^3 , can maintain pressure down to 10 Pa and can be filled with CO_2 gas. However, it runs at ambient temperature. Tests are thus performed at a higher pressure than the Martian one (2000 Pa in air and 1000 Pa in CO_2) to reproduce the same Reynolds numbers on the blades. The facility is equipped with a test bench manufactured by ISAE-SUPAERO. It is able to measure thrust and torque at rotating speeds up to 16 000 rpm independently on upper and lower rotor, by the mean of two assemblies, as seen in Figure 8. Forces are measured through load cells with thin-film strain gauges. One is placed on the movable top of the assembly to measure thrust, the second one is placed at the bottom of the rotor-motor assembly to measure torque. Electronic signal from the gauge is linearly linked to the movement of the assemblies and to the force. Calibration is performed carefully, considering the expected very low values of thrust and torque. Optimized rotors are manufactured by ISAE-SUPAERO using 3D printed molds and are made of 4-layer carbon-epoxy composite to resist to high centrifugal forces. They weigh less than 30 g.

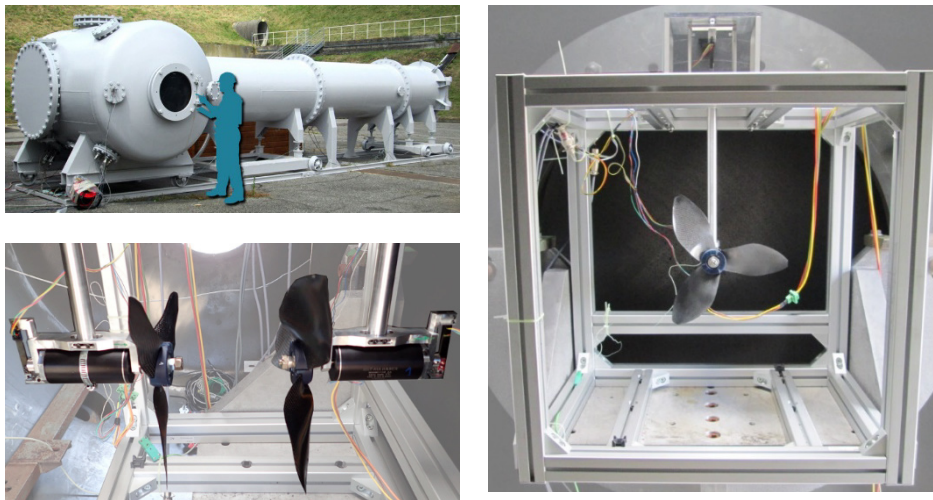


Figure 8: ONERA's low pressure tank and ISAE-SUPAERO's rotor test bench

Lots of measurements were captured but only a few are presented here. The effect of the optimization method on the aerodynamic performance is presented in Figure 9. For comparison, a standard propeller of 30 cm diameter (APC 12.25×3.75) was also tested. The optimal BEMT rotor is the one presented in section 6 (see Figure 5). The optimal FVM rotor is the upper rotor presented in section 7 (see Figure 6). Thrust and power are measured in air at low pressure and recalculated for the Martian density of 0.014 kg/m^3 . Tests were performed up to 8000 rpm. Standard propellers like APC cannot achieve enough performance for a Martian MAV: thrust is only 0.08 N at 8000 rpm and the power loading (Thrust/Power) is very low, indicating the poor efficiency of the blade. On the other hand, optimized rotors provide significant improvements. The best performance is reached through FVM optimization. Despite a larger solidity of the rotor (ratio of total blade area to the disk area), the FVM optimal rotor achieves a better power loading than the BEMT one. The goal of 0.37 N thrust (equivalent to 100 g on Mars) is reached experimentally at 7000 rpm, instead of 6100 rpm in the simulation, which means -20 % difference in thrust at equal

rotation speed. This difference may be due to slight difference in manufactured geometry and to structure deformation (twist lowered) due to centrifugal forces. The resulting power is about 10 W for 0.37 N thrust, which is quite low and accessible with a very small electric brushless motor.

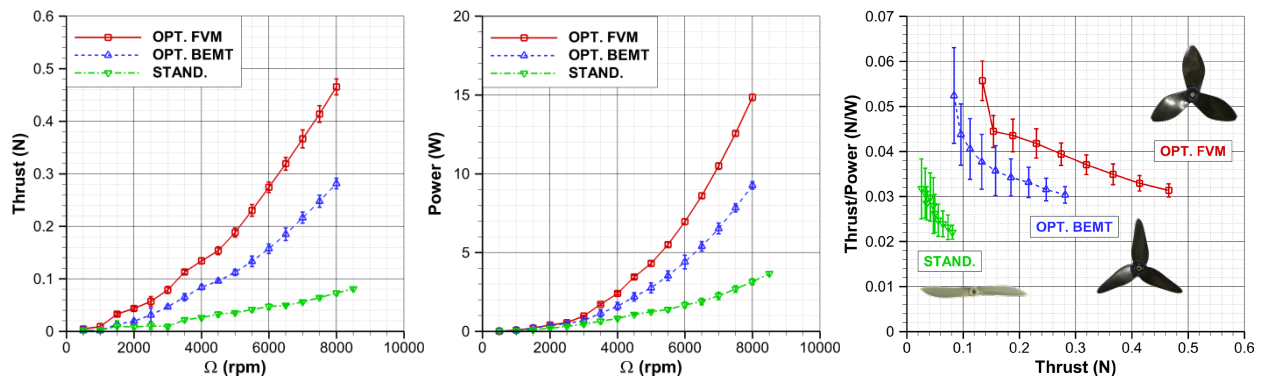


Figure 9: Effect of optimization on rotor's performance in Martian conditions

The effect of atmosphere characteristic was also questioned in the experiments. First, it is important to check if the nature of the gas, air or CO_2 , has an effect on the performance. The sound velocity differing with the gas, it is crucial to compare the results for a given tip Mach number instead of a given rotation speed. Furthermore, experiments were carried out in air and CO_2 at different pressures to maintain identical Reynolds number. To get rid of pressure influence, dimensionless parameters are formed: the thrust coefficient $C_T = T/(\rho\pi\Omega^2R^4)$ and the power coefficient $C_P = P/(\rho\pi\Omega^3R^5)$, where ρ is the density, Ω the rotation speed and R the rotor's radius (0.15 m) (SI units).

The performance of upper FVM rotor is presented in Figure 10, in terms of C_T and C_T/C_P ratio (equivalent to the power loading) versus the tip Mach number M_{tip} . The maximum rotation speed is here of 16 000 rpm, which corresponds to $M_{tip} = 0.71$ in air and $M_{tip} = 0.91$ in CO_2 . Some differences are visible, more on C_T/C_P than on C_T , and dependent on the rotation speed. It was measured very high vibration levels when rotation speed increases, coming probably from unperfected rotor's balance, which could have impacted the measure itself. However, it can be considered that the nature of the gas has little influence, in agreement with previous observations [18]. The thrust coefficient drops significantly for $M_{tip} = 0.5$, whereas C_T/C_P stays almost constant. An inflexion is visible beyond $M_{tip} = 0.7$ and the C_T/C_P ratio is surprisingly increasing, whereas one expected that transonic effects would increase drastically the power and decrease the C_T/C_P ratio. It means that the rotor can be operated over a large rotation speed range.

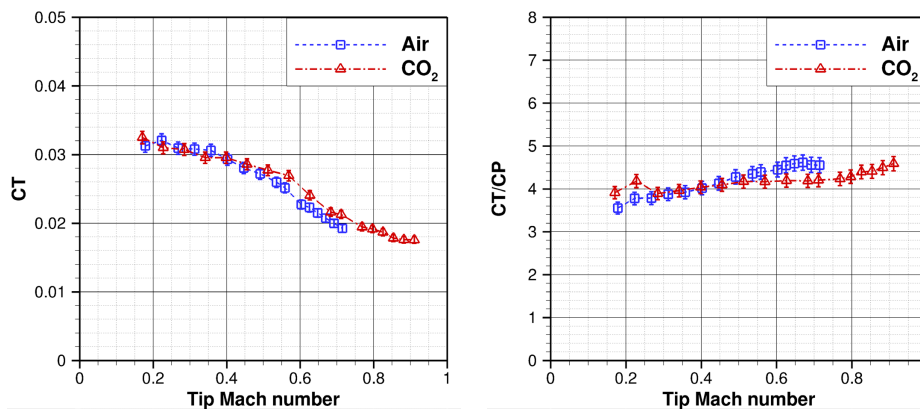


Figure 10: Effect of gas composition on the rotor's performance (FVM-optimized)

The second effect addressed here is the effect of density, or consequently the effect of the Reynolds number, by varying the tank's pressure. Tests were performed in air at ambient temperature and pressure of 20, 100, 500, 1000 hPa. These pressure values correspond on Earth to density conditions found respectively at about 30, 20, 10 and 0 km altitude. Results are presented in Figure 11. Again, it is quite surprising that the density has so little influence on the thrust and power coefficients, whereas the airfoil and the blade geometries are optimized for Reynolds numbers below 10^4 with laminar flow. Considering the blade's chord of 7 cm at $0.7R$ and a rotation speed of 4000 rpm, the chord Reynolds numbers are respectively 4000, 20 000, 90 000 and 180 000. The boundary layer flow

probably becomes turbulent above 20 000, but the rotor still exhibits a C_T value of 0.036 and a C_T/C_P ratio of 4.5, close to the values for ultra-low Reynolds numbers. This result proves again the great rotor's operability.

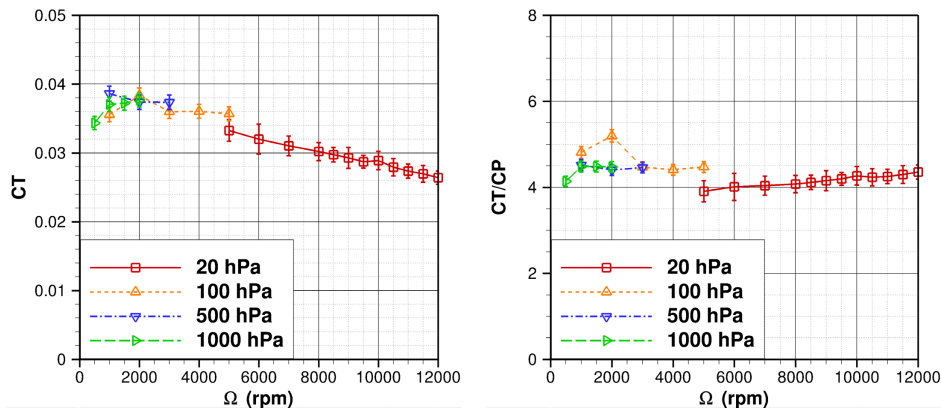


Figure 11: Effect of density on the rotor's performance (FVM-optimized)

The last effect presented here addresses the influence of the rotor's spacing on the performance of the optimized coaxial configuration. The lower rotor set-up can be placed at two different locations to provide 9 cm ($h/R = 0.6$) or 16 cm ($h/R = 1.07$) spacing between the rotors. As said before, upper and lower rotors are optimized to produce 0.37 N thrust each in Martian conditions and opposite torque. Tests are carried out as following: for each rotation speed of the upper rotor, three values of rotation speed are set for the lower rotor, and thrust and torque are measured for both rotors. Then the speed of the lower rotor is interpolated within the three values (assuming a Ω^2 behavior of the torque) so as to equal the torque of the upper rotor. Then thrust and rotation speed are deduced. The results are presented in Figure 12 for Martian conditions. The effect of the rotor spacing is very low, which confirms that coaxial rotor performance can be considered independent of spacing above $h/R = 0.4$. For 0.37 N thrust on the upper rotor, rotation speed is 6800 rpm, torque is 0.014 Nm and power is 10 W. For equal torque on the lower rotor, rotation speed is 8850 rpm, thrust is 0.31 N and power is 13 W. The total thrust is 0.69 N and not 0.74 N as expected, and the rotation difference is 2050 rpm, instead of 2400 rpm given in the simulations. It means the lower rotor produces a little too much torque from expected. To achieve a total thrust of 0.74 N, rotation speed should be 5% higher: respectively 7100 rpm and 9150 rpm for the upper and lower rotors, and the total power is only 25 W.

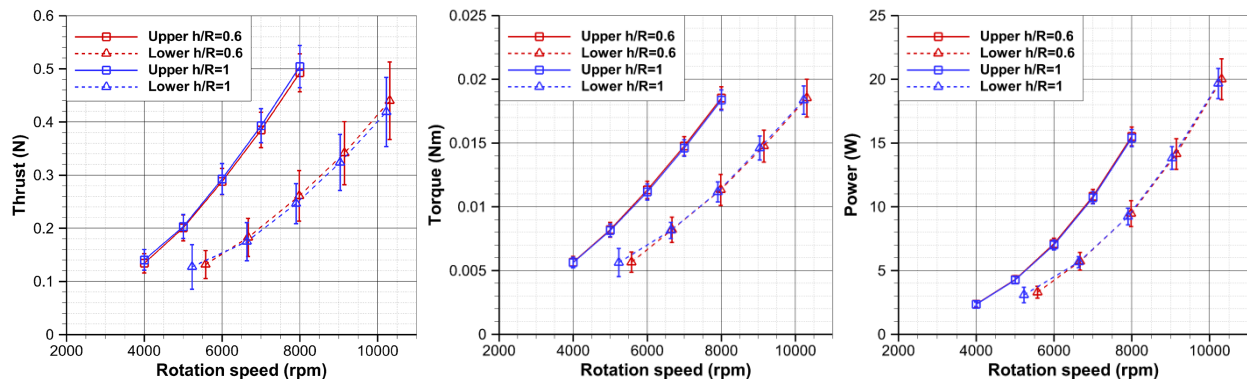


Figure 12: Effect of rotor spacing on performance of coaxial configuration in Martian conditions

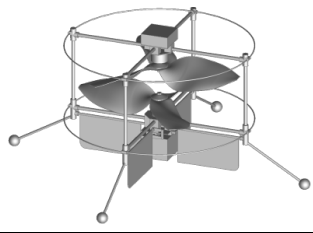
10. Preliminary design of a Martian MAV

The experimental results can be used for a preliminary design of a Martian MAV, based on existing technologies for terrestrial drones: carbon composite rotors and structure, brushless motors, electronic speed controller (ESC), LiPo battery, servomotors, flight controller, emitter-receiver, camera. The 200 g total mass of the coaxial configuration was used initially as a basis for design, but seems hardly feasible. The experimental results, expressed as C_T and C_P values, can be used at any rotation speed conditions to lift and power any prescribed mass resulting from a reasonable mass budget for the different elements of the MAV. After a few design iterations, a total mass of 400 g seems more accessible, based on the budget presented in Table 2. The MAV can be controlled laterally through two orthogonal flaps piloted by servomotors. Classical control on helicopter is made through pitch control and articulated

blade at the hub, which is hardly possible here considering the high inertia of the blades and which usually involves complex and heavy mechanical systems. The altitude and rotation of the drone can be controlled through independent management of each motor's rotation speed. Considering the Martian atmosphere's mean daytime density of 0.0167 kg/m^3 , a mass of 400 g needs about 1,5 N thrust, which can be achieved by the optimized coaxial configuration with rotation speeds of 9200 and 12 000 rpm for upper and lower rotors respectively. The corresponding power needed is 67 W. Considering a motor mechanical efficiency of 75%, a battery energy mass ratio of 160 Wh/kg and a battery managing system limiting its available capacity to 80%, a battery mass of 110 g could achieve a flight of about 9 min, which is enough to take-off, climb to a few tens meter altitude, explore the surroundings within a few hundreds meter around the rover and land.

Table 2: Mass budget (g) of a coaxial rotor Martian MAV of 400 g.

Rotors	Motors	ESC	Battery	Structure
50	60	20	110	100
Servos	Controller	Emitter	Receiver	Camera
10	20	10	10	10



11. Conclusion and perspectives

This paper shows that it is possible to design airfoils and rotors optimized for the flight of a vertical take-off and landing micro aerial vehicle in Martian atmosphere, where laminar compressible ultra-low Reynolds number flows occur. The free vortex method used in the rotor optimization process is able to accurately take into account the effect of the wake induced velocities on the rotor's performance, either in isolated or coaxial configuration. This method compares well with more advanced unsteady laminar Navier-Stokes simulations, which is not the case of the simpler blade element momentum theory. The ONERA's low pressure tank associated to the ISAE-SUPAERO's test bench provided a large data base on isolated and coaxial rotors' thrust and power capacities over a large range of rotation speeds, which confirms the efficiency of the optimized rotors. Surprisingly, the rotor stays efficient up to transonic speed at blade tip and up to ambient pressure, i.e. high Reynolds numbers. These experimental results will be deeper investigated in the future by further Navier-Stokes simulations. Additional optimizations are currently in progress: firstly, a coaxial configuration with equal rotation speeds for both rotors; secondly, a higher lift capacity coaxial configuration, typically $2 \times 300 \text{ g}$ mass in Martian gravity (2.2 N total thrust). These new optimized rotors will be manufactured and tested in the low pressure tank mid-2019. The proposed prototype needs deeper system analysis: the association motor-ESC is essential and preliminary tests with existing components show that managing such high inertia rotors is not straightforward. The concept of flaps for lateral flight control will be investigated this year by a specific set-up added in the low pressure tank. In the future, a full prototype will be manufactured and tested in Earth gravity at different pressure levels to assess the present concept of a coaxial rotor VTOL MAV for Mars exploration.

Acknowledgments

The authors would like to thank M. Saccoccio and G. Doulsier from CNES for supporting the experimental campaign, R. Chanton, H. Dedieu, S. Belliot and X. Foulquier from ISAE-SUPAERO for the rotors' production and the test bench, and C. Corato from ONERA for the facility management.

References

- [1] Balaram, J. and Tokumar, P.T. 2014. Rotorcraft for Mars exploration. In: *11th International Planetary Probe Workshop*, Pasadena, California, USA.
- [2] Bézard, H., and Moschetta, J.-M. 2015. Aerodynamic Design of a Rotary-Wing Micro Air Vehicle for Flying on Mars. In: *Space Robotics Symposium*, Glasgow, UK.
- [3] Bohorquez, F., 2007. Rotor Hover Performance and System Design of an Efficient Coaxial Rotary Wing Micro Air Vehicle. Ph.D. thesis, Maryland University.

-
- [4] Braun, R., Wright, H., Croom, M., Levine, J.S., and Spencer, D. 2006. "Design of the ARES Mars Airplane and Mission Architecture. *Journal of Spacecraft and Rockets*, 43(5).
- [5] Cambier, L., Gazaix, M., Heib, S., Plot, S., Poinot, M., Veuillot, J.-P., Boussuge, J.-F., and Montagnac, M. 2011. An overview of the multi-purpose *elsA* flow solver. *Journal Aerospace Lab*, 2:1-15.
- [6] Corfeld, K., Strawn, R., and Long, L. N. 2002. Computational Analysis of a Prototype Martian Rotorcraft Experiment. In: *20th AIAA Applied Aerodynamics Conference*, St. Louis, Missouri, USA.
- [7] Désert, T. 2019. Étude aéropulsive d'un micro-drone à voilure tournante pour l'exploration martienne. Ph.D. Thesis, ISAE-SUPAERO, Toulouse University, France.
- [8] Désert, T., Moschetta, J.-M., and Bézar, H. 2018. Numerical and experimental investigation of an airfoil design for a Martian micro rotorcraft. *International Journal of Micro Air Vehicles*, 10(3):262-272.
- [9] Drela, M. 1989. XFOIL: An Analysis and Design System for Low Reynolds Number Airfoils. *Low Reynolds Number Aerodynamics. Lect. Notes in Eng.*, 54:1-12.
- [10] Drela, M. 2007. <http://web.mit.edu/drela/Public/web/qprop>.
- [11] Kerzhanovich, V., et al. 2004. Breakthrough in Mars balloon technology. *Advances in Space Research*, 33(10).
- [12] Kunz, P.J. 2003. Aerodynamics and Design for Ultra-Low Reynolds Number Flight. Ph.D. Thesis, Stanford University, USA.
- [13] Lakshminarayan, V., and Baeder, J. 2010. Computational Investigation of Microscale Coaxial-Rotor Aerodynamics in Hovers. *Journal of Aircraft*, 47(3).
- [14] Leovy, C. 2001. Weather and climate on Mars. *Nature*, 412:245-249.
- [15] Liu, Z. 2011. Design and aero-propulsive analysis of a nano air vehicle. Ph.D. Thesis, Northwestern Polytechnical University of China, China.
- [16] Liu, Z., Albertani, R., Moschetta, J., Thipyopas, C., and Xu, M. 2011. Experimental and Computational Evaluation of Small Microcoaxial Rotor in Hover. *Journal of Aircraft*, 48(1).
- [17] Munday, P., Taira, K., Suwa, T., Numata, D., and Asai, K. 2015. Nonlinear Lift on a Triangular Airfoil in Low-Reynolds-Number Compressible Flow. *Journal of Aircraft*, 52(3):924-931
- [18] Rogers, S. E. and Kwak, D. 1990. An Upwind Differencing Scheme for the Time Accurate Incompressible Navier-Stokes Equations. *AIAA Journal*, 28(2):253-262.
- [19] Shrestha, R., Benedict, M., Hrishikeshavan, V., and Chopra, I. 2016. Hover Performance of a Small-Scale Helicopter Rotor for Flying on Mars. *Journal of Aircraft*, 53(4):1-8.
- [20] Song, H., and Underwood, C. 2007. A Mars VTOL Aerobot - Preliminary Design, Dynamics and Control. *IEEE Aerospace Conference*.
- [21] Tsuzuki, N., Sato, S. and Abe, T. 2004. Conceptual Design and Feasibility for a Miniature Mars Exploration Rotorcraft. In: *24th International Congress of the Aeronautical Sciences*.
- [22] Young, L., Derby, M., Demblewski, R., and Navarrete, J., 2002. Experimental Investigation and Demonstration of Rotary-Wing Technologies for Flight in the Atmosphere of Mars. In: *58th Annual Forum of the AHS*.